https://doi.org/10.5194/egusphere-2026-1140
Preprint. Discussion started: 5 May 2026


# Deriving the telescope focus function for a pulsed coherent Doppler lidar without a reference instrument

Pyry Pentikäinen[1], Ewan J. O'Connor[2,3], and Ronny Leinweber[4]

[1]Institute for Atmospheric and Earth System Research / Physics, Faculty of Science, University of Helsinki, Helsinki, Finland
[2]Finnish Meteorological Institute, Helsinki, Finland
[3]Department of Meteorology, University of Reading, United Kingdom
[4]Deutscher Wetterdienst, Meteorological Observatory Lindenberg – Richard Aßmann Observatory, Lindenberg, Germany

**Correspondence:** Pyry Pentikäinen (pyry.pentikainen@helsinki.fi)

**Abstract.** Obtaining profiles of attenuated backscatter coefficient from the signal-to-noise ratio measured by a pulsed coherent Doppler lidar requires knowledge of the instrument telescope focus function, which is often unknown. Here, we present a methodology for deriving the telescope focus function from horizontally-pointing pulsed coherent Doppler lidar measurements without the use of an external reference. The method relies on the assumption that the horizontal profile of attenuated backscatter coefficient is close to homogeneous, which is tested for using a convolution filter. The methodology was applied to measurements from eight co-located Doppler lidars and the results compared to a methodology for deriving the telescope focus function using vertically-pointing Doppler lidar measurements using an elastic backscatter lidar as reference. The telescope focus functions obtained with the two methodologies show good agreement even for measurement periods as short as two days.

## 1 Introduction

Pulsed coherent Doppler lidars simultaneously measure the radial Doppler velocity and the signal-to-noise ratio (SNR) of the backscattered signal. For Doppler lidars with scanning ability, the vertical and horizontal wind vector components can be derived from the radial Doppler velocities through the application of appropriate trigonometric functions if the wind field can be considered to be homogeneous (Browning and Wexler, 1968; Lane et al., 2013; Päschke et al., 2015; Mariani et al., 2020). However, to retrieve the profile of the attenuated backscatter coefficient, $\beta'$, from the profile of SNR requires knowledge of the telescope focus function ($T_\mathrm{f}$) for the Doppler lidar, which varies non-linearly with the measurement range. If $T_\mathrm{f}$ is known or can be calculated (Chouza et al., 2015; Pentikäinen et al., 2020), then the profile of $\beta'$ can be derived making it possible to use the Doppler lidar as an elastic backscatter lidar. This can lead to cost reductions for measurement campaigns that require both wind and attenuated backscatter coefficient profiles, or enable a Doppler lidar to be used as a backup instrument for an elastic backscatter lidar. However, for most scanning Doppler lidars, $T_\mathrm{f}$ is unknown or deviates significantly from what is assumed, which prevents the accurate calculation of the profile of $\beta'$.

Attenuated backscatter observations from elastic backscatter lidars are used for assessing air quality (Diémoz et al., 2019), detecting cloud base heights (Platt et al., 1994), retrieving the atmospheric boundary layer height (Dang et al., 2019; Kotthaus

https://doi.org/10.5194/egusphere-2026-1140
Preprint. Discussion started: 5 May 2026


et al., 2023), and used for validating chemical transport models by using attenuated backscatter forward modelling (Geisinger et al., 2017). There is also potential for assimilating attenuated backscatter into the numerical weather prediction models (Warren et al., 2022). Petters et al. (2024) used the fluctuations in Doppler lidar vertical velocities and attenuated backscatter coefficient to derive aerosol fluxes for particles larger than 0.53 $\mu$m. The attenuated backscatter coefficients were calculated using a factory calibration (Newsom and Krishnamurthy, 2022), which however does not correspond the actual $T_{\mathrm{f}}$. They limited the flux calculations to only one height, which still permitted a consistent estimate of the aerosol fluxes. However, the obtained empirical correlations between backscatter and aerosol number concentration are not applicable to other heights or other Doppler lidar units.

The attenuated backscatter profile can also be used for detection of cloud phase by calculating the integrated lidar ratio from fully attenuating cloud layers. Liquid cloud layers have a specific integrated lidar ratio at certain wavelengths, which can also be used for calibrating ceilometers (O'Connor et al., 2004; Hopkin et al., 2019). Although there is limited information on the lidar ratios for clouds at wavelengths above 1 $\mu m$ (Petters et al., 2024), lidar ratio values for liquid clouds at 1.53$\mu m$ have been calculated and observed (Westbrook et al., 2010) and so obtaining the cloud phase should be possible from $T_{\mathrm{f}}$ corrected coherent Doppler lidars. This could have great potential for the wind energy sector where Doppler lidars are already commonly used for wind resource assessments (Liu et al., 2019). Considering the significance of icing on wind turbine's energy production (Bredesen et al., 2017) and safety (Krenn et al., 2022) in cold climates, site specific validation of icing models (Hämäläinen et al., 2020) with a Doppler lidar during wind resource assessment measurements could have significant financial benefits.

In this paper we present a method for deriving the $T_{\mathrm{f}}$ for pulsed coherent Doppler lidars which requires no additional devices as reference. The method is based on using horizontally pointing Doppler lidar measurements for which the along beam backscatter profile is often approximately homogeneous. The method is tested with 8 co-located pulsed coherent Doppler lidars and compared to another $T_{\mathrm{f}}$ retrieval method based on using a co-located ceilometer as a reference instrument (Pentikäinen et al., 2020).The measurement site and the used Doppler lidars and ceilometer elastic backscatter lidar are described in Section 2. $T_{\mathrm{f}}$ and the methodologies for deriving it are presented in Section 3. The obtained $T_{\mathrm{f}}$ and associated uncertainties for the 8 Doppler lidars and the comparison of the two methods for deriving $T_{\mathrm{f}}$ are shown in Section 4. Conclusions are given in Section 5.

## 2 Data

### 2.1 Site

The data used for this study was gathered during the FESSTVaL (Field Experiment on submesoscale spatio-temporal variability in Lindenberg) campaign (FESSTVaL team, 2023), in Lindenberg, Germany. The campaign took place during the summer months of 2021, with the data used here being collected during 19th to 25th July. During this time period 8 closely located Doppler lidars measured simultaneously in the vertical and at 5° elevation angle (85° zenith) at Falkenberg, about 5 km from Lindenberg . Measurements from a collocated CHM 15k ceilometer are also available.

https://doi.org/10.5194/egusphere-2026-1140
Preprint. Discussion started: 5 May 2026


**Figure 1.** Eight Doppler lidars and a ceilometer operating in the same location at Falkenberg, Germany, during the FESSTVAl Campaign. Photo courtesy of Ronny Leinweber.

All of the instruments were located at 52.167°N, 14.123°E. The surroundings consist mainly of flat fields with some interspersed trees. Figure 1 shows how the instruments were deployed.

### 2.2 Doppler lidar

The 8 Doppler lidars in the FESSTVaL campaign comprise both Halo Photonics Streamline, and Streamline XR versions. These are commercially available heterodyne pulsed systems capable of full-hemispheric scanning and operated at a temporal resolution of 1-2 s (see Table 1). The focus for the Streamline version can be set by the operator, whereas for the Streamline XR the focus is set by the manufacturer.

https://doi.org/10.5194/egusphere-2026-1140
Preprint. Discussion started: 5 May 2026


**Table 1.** Halo Photonics Streamline and Streamline XR heterodyne Doppler lidar specifications.

| | |
|---|---|
| Wavelength | 1.5 $\mu$m |
| Pulse repetition rate | 10 or 15 kHz |
| Nyquist velocity | 19.8 m s$^{-1}$ |
| Sampling frequency | 50 MHz |
| Points per range gate | 10 / 16 |
| Range resolution | 30 m / 48 m |
| Pulse duration (Streamline systems) | $166 - 214$ ns |
| Pulse duration (Streamline XR systems) | $330 - 414$ ns |
| Divergence | 33 $\mu$rad |
| Antenna | monostatic optic-fibre coupled |

### 2.3 Ceilometer

The CHM15k Nimbus ceilometer is a single channel elastic backscatter lidar operating at a wavelength of 1064 nm and manufactured by Lufft Mess- und Regeltechnik GmbH. It has a biaxial system with the Nd:YAG transmitter having a pulse repetition rate of 5-7 kHz and an avalanche photodiode operating in photon counting mode (Wiegner and Geiß, 2012; Madonna et al., 2015). Full overlap between transmitter and the telescope is achieved at about 800 m in range (Hervo et al., 2016), and the instrument was operated during this campaign with a time resolution of 15 seconds and a range resolution of 15 m up to 15 km.

## 3 Methodology

### 3.1 Telescope focus function

The coherent Doppler lidar equation is given by (Frehlich and Kavaya, 1991)

$$\mathrm{SNR}(R) = \frac{\eta c E}{2h\nu B} \frac{A_e(R)}{R^2} \beta'(R), \tag{1}$$

where $\beta'$ is the attenuated backscatter coefficient, $\eta$ is the detector quantum efficiency, $c$ is the speed of light, $E$ is the beam energy, $h$ is Planck's constant, $\nu$ is the optical frequency, $A_\mathrm{e}(R)$ is the $1/e^2$ effective receiver area and $R$ is range, and $B$ is the receiver bandwidth.

https://doi.org/10.5194/egusphere-2026-1140
Preprint. Discussion started: 5 May 2026


For a monostatic system emitting a circular Gaussian beam, using a circular aperture, and having matched filters, the effective receiver area is given by (Frehlich and Kavaya, 1991; Henderson et al., 2005)

$$A_e(R) = \frac{\pi D^2}{4\left(1 + \left(\frac{\pi D^2}{4\lambda R}\right)^2 \left(1 - \frac{R}{f}\right)^2 + \left(\frac{D}{2\rho_0}\right)^2\right)}, \tag{2}$$

where $D$ is the $1/e^2$ effective diameter of a Gaussian beam, $\lambda$ is the laser wavelength, $f$ is the effective focal length of the telescope for the transmitter and receiver, and $\rho_0$ is a turbulence parameter, also termed transverse field coherence length.

The range dependent terms in Eq. (1) can be written as an unitless telescope focus function

$$T_\mathrm{f} = \frac{A_\mathrm{e}(R)}{R^2}, \tag{3}$$

where $T_\mathrm{f}$ is the telescope focus function. If $T_\mathrm{f}$ is known, profiles of $\beta'$ can be calculated from the SNR using 1.

Pentikäinen et al. (2020) showed that the influence of refractive turbulence is small and $\rho_0 \to \infty$ can be assumed when operating the Doppler lidar pointing vertically. Hence, the term $\left(\frac{D}{2\rho_0}\right)^2$ in Eq. 2 can be neglected, which allows for the derivation of $T_\mathrm{f}$ (see Section 3.2).

When operating a coherent lidar horizontally, the impact of refractive turbulence is much more significant. Estimating $\rho_0$ simultaneously with $f$ and $D$ may be possible by assuming $\rho_0$ is homogeneous along the lidar beam path, but the introduction of a third variable into the estimation procedure increases the calculation time significantly. The validity of assuming $\rho_0$ as homogeneous is also questionable close to the surface, where local variations in the surface properties can produce significant variations along the beam path. Alternatively, the data used for the estimation $f$ and $D$ can be limited to moments of time when $\rho_0 \to \infty$ is a reasonable assumption. This can be achieved with a threshold value for a maximum allowed deviation between the corrected measurement profile and the reference profile in the $T_\mathrm{f}$ fitting procedure. Deriving $\rho_0$ from measurements of refractive index by scintillometry or model data may also be a viable option.

### 3.2 Vertical method

The methodology for deriving $T_\mathrm{f}(R)$ using a collocated ceilometer is described in Pentikäinen et al. (2020). The methodology consists of two main steps, filtering and iterative fitting procedure. The filtering step ensures that the data from the Doppler lidar and ceilometer are comparable to each other and that each profile consists of a sufficient amount of usable data points. The data from both the Doppler lidar and the ceilometer is normalized prior to the comparison, and hence the differences in the absolute values between the two instruments pose no issue, it is important that there remains a linear relationship between the values in both measurements. This condition is crucial due to the typically different wavelengths used by Doppler lidars and ceilometers, which respond differently to changes in the aerosol composition and hydrometeors. Additionally, parts of the ceilometer profile that are affected by the overlap function and not properly corrected for have to be discarded. Here, the ceilometer data was corrected for the overlap function, and data above 330 m agl. was considered to be usable, with heights below this being discarded.

https://doi.org/10.5194/egusphere-2026-1140
Preprint. Discussion started: 5 May 2026


The fitting procedure consists of iteratively applying different $T_f(R)$ from a preselected parameter space of $f$ and $D$, and calculating the mean square errors (MSE) between the generated Doppler lidar profiles and the ceilometer attenuated backscatter profiles. The parameters producing the smallest MSE are then chosen as the best estimate for that profile. Repeating this procedure for a large number of profiles produces a two dimensional Gaussian distribution for $D$ and $f^{-2}$, from which $T_f(R)$ and its uncertainty can be estimated.

Due to having only a couple days of data where all eight Doppler lidars were measuring in vertical staring mode simultaneously, the temporal averaging period of the data was reduced to 1 minute from the 30 minute averaging period used by Pentikäinen et al. (2020) to increase the amount of data points in the $(f^{-2}, D)$ distribution.

### 3.3 Horizontal method

Derivation of $T_f(R)$ from horizontal measurements bypasses the need of a reference elastic backscatter lidar by assuming that the aerosol composition in the boundary layer is close to homogeneous for a significant portion of the time. During these time periods backscatter is nearly constant along the lidar beam, resulting in SNR taking the shape of $T_f(R)$ with minor variations due to the instrument sensitivity, refractive turbulence, and attenuation.

For an accurate estimate of $T_f(R)$, it is important that the assumption of near horizontal homogeneity of $\beta'$ is valid. Data deviating significantly from this assumption are filtered out using a convolution filter, where large step changes in the SNR profile are detected with a convolution using a four range gate long Haar-wavelet. The Haar-wavelet was chosen due to its robustness in detecting step changes in the analysed signal. The shape of $T_f(R)$, which is should remain in the data after filtering, changes smoothly, while aerosol plumes, that break the assumption of homogeneity and should be removed, can create strong step changes.

The filtering is based on a threshold for the result of the convolution. Sensitivity tests were performed for the decision of the threshold to allow for the variation in the $T_f(R)$ and some additional normally distributed variance in noise and $\beta'$. Reasonable $T_f(R)$ can triple with a distance of 100 m, and considering the SNR values observed in the used measurement period a threshold on of $\pm$ 0.5 was chosen. This corresponds to a 0.375 linear change in SNR over a length of the wavelet. All data beyond the first instance where the threshold is exceeded are removed. The simple threshold method presented here can be used for short measurement periods of a few days when there is not much variation in the overall SNR levels. Given a longer measurement period with more variation in the SNR, a proportional threshold would be more appropriate.

The convolution filter ensures that if step changes in aerosol properties exist along the profile, all data beyond the point where the first change occurs are discarded. All data beyond the first range gate influenced significantly by noise are also removed at the same time. After this filtering, profiles with eight or more range gates of data remaining are used for fitting of the $T_f(R)$ parameters.

The fitting procedure for the $T_f(R)$ parameters is similar to the vertical method, except that the normalised profiles are compared to unity instead of the normalised attenuated backscatter profile from an elastic backscatter lidar.

Two estimates for $T_f(R)$ were produced from the near horizontal staring mode; with and without filtering based on the MSE calculated during the fitting procedure. The MSE filtering removes estimates with too high uncertainty from the $(f^{-2}, D)$

https://doi.org/10.5194/egusphere-2026-1140
Preprint. Discussion started: 5 May 2026


distribution, and is especially important for the horizontal measurements due to the possible impact of $\rho_0$. Section 4.3 shows that higher values of $\left(\frac{D}{2\rho_0}\right)^2$ are likely linked with higher MSE in the fitting procedure. As the fitting procedure assumes no refractive turbulence, the estimates from moments of time with high $\left(\frac{D}{2\rho_0}\right)^2$ are likely to distort the results.

## 4 Results

### 4.1 Parameter estimates

Estimates of $f$ and $D$ for all 8 Doppler lidars with the vertical method, the horizontal method, and the horizontal method with MSE filtering are given in Table 2. The corresponding $T_\mathrm{f}$ are visualised in Figure 2.

The different methods agree generally well. For Doppler lidars nrs. 74, 172, and 177 (all Streamline systems with the capability of changing focus) the difference in $D$ obtained with the vertical and horizontal methods is larger than the calculated uncertainty (one standard deviation). This indicates that the length of the available data period may not be long enough for accurate assessment of the uncertainty. However, the difference may also be explained by slight deviations in the telescope geometry occurring during change of the elevation angle, which could result in the laser beam properties not matching the assumptions in 2.

For most of the analysed Doppler lidars, the estimated values of $D$ and $f$ remain the same whether or not the MSE filter is applied to the horizontal results. Large deviations are seen only with Doppler lidar nrs. 143 and 146, for which the MSE filter removes significant proportion of the data. This indicates that either the sensitivity of Doppler lidar nrs. 143 and 146 vary from the rest of the analysed Doppler lidars, or that they may have some issues in the telescope geometry.

For Doppler lidar nr. 143 the MSE filtered results matches better with the vertical method than the horizontal method without the filter does. This may indicate that the data filtered out by the convolution would distort the results away from the true values of $D$ and $f$ if it remained in the used data set.

For Doppler lidar nr. 146 the convolution filtering removes all but a few individual profiles of data, resulting in the final MSE filtered estimate being made with only a small amount of data. This may explain the differences seen in the results between the MSE filtered horizontal method and the other methods.

The uncertainty of each $T_\mathrm{f}$ estimate in the corrected $\beta'$ profiles is given in Table 3. The uncertainty is given as the maximum value for the whole profile. Note, that the uncertainty for most parts of the profile is lower than this, as is shown in Pentikäinen et al. (2020). The uncertainties are estimated by re-sampling as described in Pentikäinen et al. (2020).

### 4.2 Comparison of derived attenuated backscatter profiles

Visualisations of the $\beta'$ calculated with $T_\mathrm{f}$ obtained from the vertical method and the MSE filtered horizontal method are presented in Figure 3. The $\beta'$ calculated with the $T_\mathrm{f}$ assumed by operator of the device is shown if Figure 3a, the $\beta'$ calculated with the $T_\mathrm{f}$ obtained with the vertical and the MSE filtered horizontal methods are shown respectively in Figures 3b and 3c, and the $\beta'$ from the collocated elastic backscatter lidar in Figure 3d. Significant differences are seen between the $\beta'$ based on

https://doi.org/10.5194/egusphere-2026-1140
Preprint. Discussion started: 5 May 2026


**Table 2.** Estimates of $f$ and $D$ for all lidar for vertical data, horizontal data and horizontal data with MSE filtered results.

| | Vertical | | Horizontal | | Horizontal MSE filtered | |
|---|---|---|---|---|---|---|
| Doppler lidar nr. | $f$ (m) | $D$ (mm) | $f$ (m) | $D$ (mm) | $f$ (m) | $D$ (mm) |
| 44 | $425 \pm 109$ | $13.3 \pm 1.8$ | $465 \pm 30$ | $14.2 \pm 0.4$ | $465 \pm 28$ | $14.2 \pm 0.4$ |
| 74 | $415 \pm 18$ | $20.0 \pm 0.7$ | $415 \pm 16$ | $22.0 \pm 1.1$ | $415 \pm 6$ | $22.0 \pm 0.4$ |
| 78 | $1690 \pm 600$ | $22.5 \pm 0.7$ | $1330 \pm 709$ | $22.5 \pm 1.0$ | $1300 \pm 128$ | $23.0 \pm 1.0$ |
| 143 | inf | $15.3 \pm 1.0$ | inf | $12.8 \pm 2.4$ | inf | $15.8 \pm 0.8$ |
| 146 | $485 \pm 34$ | $16.5 \pm 1.3$ | $490 \pm 22$ | $16.5 \pm 0.4$ | $535 \pm 47$ | $15.5 \pm 0.7$ |
| 161 | inf | $16.0 \pm 1.1$ | inf | $16.0 \pm 0.7$ | inf | $16.0 \pm 0.7$ |
| 172 | $930 \pm 384$ | $21.8 \pm 1.0$ | $920 \pm 59$ | $23.3 \pm 0.7$ | $920 \pm 46$ | $23.3 \pm 0.5$ |
| 177 | $420 \pm 21$ | $21.5 \pm 0.8$ | $435 \pm 11$ | $22.8 \pm 0.7$ | $435 \pm 9$ | $22.8 \pm 0.5$ |

**Table 3.** Estimates of maximum $\beta'$ uncertainty for each method and Doppler lidar.

| Doppler lidar nr. | Vertical | Horizontal | Horizontal MSE filtered |
|---|---|---|---|
| 44 | 40 % | 6 % | 6 % |
| 74 | 8 % | 11 % | 4 % |
| 78 | 82 % | 97 % | 10 % |
| 143 | 28 % | 59 % | 11 % |
| 146 | 17 % | 6 % | 12 % |
| 161 | 15 % | 10 % | 10 % |
| 172 | 22 % | 7 % | 6 % |
| 177 | 11 % | 7 % | 6 % |

the assumed and derived $T_{\mathrm{f}}$. The former shows a band of high values near the surface and a strong decrease with height, while the latter matches very closely with the elastic backscatter lidar with a close to uniform backscatter throughout the boundary layer. The $\beta'$ using the vertical and the horizontal MSE filtered method match very well, indicating that even though there is a 40 m difference in the derived $f$ and 0.9 mm difference in the derived $D$, the impact of these variations on the $\beta'$ profiles is relatively small.

Figure 4 shows the median deviation between $\beta'$ from the ceilometer and normalized $\beta'$ from the Doppler lidar as a function of range. The normalization of the Doppler lidar $\beta'$ is done at the range between 345 m and 885 m. The data was averaged to 1 hour resolution before calculation of the deviation. The deviations are the smallest for the vertical $T_{\mathrm{f}}$ estimates, as is expected since they were obtained from the same data and by comparison to the same ceilometer. However, this does not indicate that

https://doi.org/10.5194/egusphere-2026-1140
Preprint. Discussion started: 5 May 2026


the vertical $T_\mathrm{f}$ estimation method is the most accurate, as whether the difference can also be a result of artefacts arising from the overlap correction of the ceilometer.

For most of lidars the deviation trends towards negative values beyond 1000 m, indicating that $\beta'$ from the Doppler lidar is larger than from the ceilometer. This may be caused by the Doppler lidar background noise being multiplied by the inverse of $T_\mathrm{f}$ during the correction process, which can result in artificially increased values beyond the apparent focus, especially if the SNR is small in relation to the actual variation in the noise.

Additionally, Figure 4 shows that $\beta'$ from Doppler lidar nr. 146 deviates significantly from the other Doppler lidars beyond 800 m. The reason for this behaviour is unclear.

### 4.3 Influence of attenuation and refractive turbulence

The influence of refractive turbulence on the deriving $T_\mathrm{f}(R)$ from vertically pointing data was evaluated in Pentikäinen et al. (2020), and the effect was deemed small. For measurements in the horizontal, the influence of refractive turbulence is significantly higher and attenuation is also often larger than in the vertical. A four parameter fitting procedure was applied to the FESSTVaL data to test whether attenuation and $\rho_0$ could be derived simultaneously with $f$ and $D$. Both attenuation and $\rho_0$ were assumed constant along the beam to simplify the fitting. However, the resulting estimates were not consistent between different Doppler lidar units and the results are thus not considered reliable.

Despite not being able to quantify attenuation and $\rho_0$ from the data, their influence on the fitting procedure can be still inferred from fitting procedure of the estimating $f$ and $D$. Figure 5 shows the MSE between SNR profiles corrected with the best estimate $T_\mathrm{f}$ and unity as a function of time of day for all analysed Doppler lidars. The data has been averaged to 2 h resolution.

For almost all Doppler lidar units a clear diurnal pattern is visible, with higher values during daytime than at night. This coincides with the expected pattern of refractive turbulence in July and also the observed dissipation rate of TKE in the Doppler lidar data. For measurements performed at another time of the year the diurnal pattern is likely to be different.

While attenuated backscatter is not directly comparable to attenuation, the diurnal pattern of attenuated backscatter in a single range gate should give some indication of the how the attenuation of the signal should vary in the horizontal direction. Based on all Doppler lidars, the attenuation should be the smallest around 12:00 UTC and largest between 4:00 and 6:00 UTC. As the diurnal pattern deviates significantly from this assumption, it seems that the influence of refractive turbulence is more significant on the quality of the $T_\mathrm{f}$ fitting. It must be noted that the time period studied here is short and limited to only one location, so it is not possible to determine whether this conclusion is representative of general conditions. However, this seems to indicate that highly turbulent periods are not suitable for the horizontal $T_\mathrm{f}$ estimation method, as the uncertainty from to assuming $\rho_0 \to \infty$ may increase significantly.

Besides the diurnal patterns, Figure 5 shows that there are large differences in the general level of MSE for the fitting of $T_\mathrm{f}$. We assume these differences are mainly caused by differences in the sensitivity between different instruments, degradation of the instruments and non optimal alignment of the lasers.

https://doi.org/10.5194/egusphere-2026-1140
Preprint. Discussion started: 5 May 2026


## 5 Conclusions

A method for deriving $T_\mathrm{f}$ for a coherent Doppler lidar from horizontal measurements is presented. The method is tested with 8 Doppler lidars located in close proximity to each other and compared against $T_\mathrm{f}$ derived from vertical Doppler lidar measurements with the aid of a co-located ceilometer.

Good agreement in the derived $T_\mathrm{f}$ from the horizontal and vertical measurements is seen even with short measurement periods of just 2–3 days. For 7 out of the 8 Doppler lidars, the difference in the derived $f$ between the different methods is less than 50 m. For $D$, the differences are less than 2 mm for all devices. When using the derived $T_\mathrm{f}$ to calibrate a Doppler lidar for measuring $\beta'$ operationally, longer measurement period is recommended to reduce the associated uncertainties.

Uncertainties for each derived $T_\mathrm{f}$ are assessed and large variation between different Doppler lidars are seen. This is suspected to be due to differences in the sensitivities of the instruments (Päschke and Detring, 2024) as well as the level of compliance between the laser geometries of each instrument and the assumptions of the used coherent lidar equation. The horizontal method with MSE filtering has the lowest uncertainties varying from 6 m to 128 m for $f$ and from 0.4 mm to 1.0 mm for $D$, resulting in 4 % and 12 % maximum uncertainty in the $T_\mathrm{f}$. For the horizontal method without the MSE filtering the maximum $T_\mathrm{f}$ uncertainties vary from 6 % to 97 %, and for the vertical method from 8 % to 82 %.

The horizontal method for deriving $T_\mathrm{f}$ is much more susceptible to refractive turbulence than the vertical method, due to refractive turbulence decreasing often quite rapidly with height. The horizontal method requires filtering of periods with high refractive turbulence, which was implemented by using a threshold value for MSE of the $T_\mathrm{f}$ fit on the measurement data. This filtering removed mostly daytime data which matches the assumption of higher refractive turbulence during the daytime convective boundary layer.

*Data availability.* The data from the eight Doppler lidars are available from the Finnish Meteorological Institute (https://doi.org/10.57707/fmi-b2share.qssxd-qxt78, Leinweber and O'Connor, 2026).

*Author contributions.* PP developed the methodology and performed the analysis. EJO supervised the project. RL was responsible for setting up all Doppler lidar systems in FESSTVal, designing and implementing suitable scanning routines for this study, and managing the data. PP and EJO conceptualised the project and wrote the manuscript.

*Competing interests.* The authors declare that they have no conflict of interest.

https://doi.org/10.5194/egusphere-2026-1140
Preprint. Discussion started: 5 May 2026


*Acknowledgements.* This research was funded by the Vilho, Yrjö and Kalle Väisälä Foundation. We are very grateful to Frank Beyrich for organising the Doppler lidar contributions to the FESSTVal campaign and for providing comments on the draft manuscript. We also acknowledge the FESSTVAL team and the institutions who deployed the Doppler lidars for the FESSTVal campaign.

https://doi.org/10.5194/egusphere-2026-1140
Preprint. Discussion started: 5 May 2026


## References

Bredesen, R. E., Cattin, R., Clausen, N.-E., Davis, N., Jordaens, P. J., Khadiri-Yazami, Z., Klintström, R., Krenn, A., Lehtomäki, V., Ronsten, G., Wadham-Gagnon, M., and Wickman, H.: Recommended practices 13 2nd Edition: Wind energy projects in cold climates, Tech. rep., IEA Wind TCP), https://iea-wind.org/wp-content/uploads/2021/09/2017-IEA-Wind-TCP-Recommended-Practice-13-2nd-Edition-Wind-Energy-in-Cold-Climates.pdf, 2017.

Browning, K. A. and Wexler, R.: The Determination of Kinematic Properties of a Wind Field Using Doppler Radar, J. Appl. Meteor. Climatol., 7, 105 – 113, https://doi.org/10.1175/1520-0450(1968)007<0105:TDOKPO>2.0.CO;2, 1968.

Chouza, F., Reitebuch, O., Groß, S., Rahm, S., Freudenthaler, V., Toledano, C., and Weinzierl, B.: Retrieval of aerosol backscatter and extinction from airborne coherent Doppler wind lidar measurements, Atmos. Meas. Tech., 8, 2909–2926, https://doi.org/10.5194/amt-8-2909-2015, 2015.

Dang, R., Yang, Y., Hu, X.-M., Wang, Z., and Zhang, S.: A Review of Techniques for Diagnosing the Atmospheric Boundary Layer Height (ABLH) Using Aerosol Lidar Data, Remote. Sens., 11, https://doi.org/10.3390/rs11131590, 2019.

Diémoz, H., Barnaba, F., Magri, T., Pession, G., Dionisi, D., Pittavino, S., Tombolato, I. K. F., Campanelli, M., Della Ceca, L. S., Hervo, M., Di Liberto, L., Ferrero, L., and Gobbi, G. P.: Transport of Po Valley aerosol pollution to the northwestern Alps – Part 1: Phenomenology, Atmos. Chem. Phys., 19, 3065–3095, https://doi.org/10.5194/acp-19-3065-2019, 2019.

FESSTVaL team: Final Report on Field Experiment on Sub-mesoscale Spatio-Temporal Variability in Lindenberg (FESSTVaL), Tech. rep., A joint project within the Hans-Ertel Center for Weather Research Phase 3, https://fesstval.de/fileadmin/user_upload/fesstval/Files/FESSTVaL-Report-final.pdf, 2023.

Frehlich, R. G. and Kavaya, M. J.: Coherent laser radar performance for general atmospheric refractive turbulence, Appl. Opt., 30, 5325–5352, https://doi.org/10.1364/AO.30.005325, 1991.

Geisinger, A., Behrendt, A., Wulfmeyer, V., Strohbach, J., Förstner, J., and Potthast, R.: Development and application of a backscatter lidar forward operator for quantitative validation of aerosol dispersion models and future data assimilation, Atmos. Meas. Tech., 10, 4705–4726, https://doi.org/10.5194/amt-10-4705-2017, 2017.

Henderson, S. W., Gatt, P., Rees, D., and Huffaker, R. M.: Wind Lidar, in: Laser Remote Sensing, edited by Fujii, T. and Fukuchi, T., pp. 469–722, CRC Taylor and Francis, 2005.

Hervo, M., Poltera, Y., and Haefele, A.: An empirical method to correct for temperature-dependent variations in the overlap function of CHM15k ceilometers, Atmos. Meas. Tech., 9, 2947–2959, https://doi.org/10.5194/amt-9-2947-2016, 2016.

Hopkin, E., Illingworth, A. J., Charlton-Perez, C., Westbrook, C. D., and Ballard, S.: A robust automated technique for operational calibration of ceilometers using the integrated backscatter from totally attenuating liquid clouds, Atmos. Meas. Tech., 12, 4131–4147, https://doi.org/10.5194/amt-12-4131-2019, 2019.

Hämäläinen, K., Hirsikko, A., Leskinen, A., Komppula, M., O'Connor, E. J., and Niemelä, S.: Evaluating atmospheric icing forecasts with ground-based ceilometer profiles, Meteor. Appl., 27, e1964, https://doi.org/10.1002/met.1964, 2020.

Kotthaus, S., Bravo-Aranda, J. A., Collaud Coen, M., Guerrero-Rascado, J. L., Costa, M. J., Cimini, D., O'Connor, E. J., Hervo, M., Alados-Arboledas, L., Jiménez-Portaz, M., Mona, L., Ruffieux, D., Illingworth, A., and Haeffelin, M.: Atmospheric boundary layer height from ground-based remote sensing: a review of capabilities and limitations, Atmos. Meas. Tech., 16, 433–479, https://doi.org/10.5194/amt-16-433-2023, 2023.

https://doi.org/10.5194/egusphere-2026-1140
Preprint. Discussion started: 5 May 2026


Krenn, A., Stökl, A., Rodriguez, H., Schürmann, G., Weidl, T., Jenssen, U., Bredesen, R. E., Ingebrigsten, K.-O., Derrick, A., Hahm, T., Mäusling, S., Cromm, N., and Lautenschlager, F.: International Recommendations for Ice Fall and Ice Throw Risk Assessments, Tech. rep., IEA Wind TCP Task 19), https://iea-wind.org/wp-content/uploads/2022/09/Task-19-Technical-Report-on-International-Recommendations-for-Ice-Fall-and-Ice-Throw-Risk-Assessments.pdf, 2022.

Lane, S., Barlow, J., and Wood, C.: An assessment of a three-beam Doppler lidar wind profiling method for use in urban areas, Journal of Wind Engineering and Industrial Aerodynamics, 119, 53–59, https://doi.org/https://doi.org/10.1016/j.jweia.2013.05.010, 2013.

Leinweber, R. and O'Connor, E.: Doppler lidar data from Falkenberg for Pentikäinen et al. (2026) "Deriving the telescope focus function for a pulsed coherent Doppler lidar without a reference instrument". Compiled by E. O'Connor. Finnish Meteorological Institute [Data set], https://doi.org/10.57707/fmi-b2share.qssxd-qxt78, 2026.

Liu, Z., Barlow, J. F., Chan, P.-W., Fung, J. C. H., Li, Y., Ren, C., Mak, H. W. L., and Ng, E.: A Review of Progress and Applications of Pulsed Doppler Wind LiDARs, Remote. Sens., 11, https://doi.org/10.3390/rs11212522, 2019.

Madonna, F., Amato, F., Vande Hey, J., and Pappalardo, G.: Ceilometer aerosol profiling versus Raman lidar in the frame of the INTERACT campaign of ACTRIS, Atmos. Meas. Tech., 8, 2207–2223, https://doi.org/10.5194/amt-8-2207-2015, 2015.

Mariani, Z., Crawford, R., Casati, B., and Lemay, F.: A Multi-Year Evaluation of Doppler Lidar Wind-Profile Observations in the Arctic, Remote. Sens., 12, https://doi.org/10.3390/rs12020323, 2020.

Newsom, R. and Krishnamurthy, R.: Doppler Lidar (DL) Instrument Handbook, DOE/SC-ARM-TR-101, U.S. Department of Energy, Atmospheric Radiation Measurement user facility, Richland, Washington, https://doi.org/10.2172/1034640, 2022.

O'Connor, E. J., Illingworth, A. J., and Hogan, R. J.: A technique for autocalibration of cloud lidar, J. Atmos. Oceanic Technol., 21, 777–786, https://doi.org/10.1175/1520-0426(2004)021<0777:ATFAOC>2.0.CO;2, 2004.

Päschke, E. and Detring, C.: Noise filtering options for conically scanning Doppler lidar measurements with low pulse accumulation, Atmos. Meas. Tech., 17, 3187–3217, https://doi.org/10.5194/amt-17-3187-2024, 2024.

Päschke, E., Leinweber, R., and Lehmann, V.: An assessment of the performance of a 1.5 $\mu m$ Doppler lidar for operational vertical wind profiling based on a 1-year trial, Atmos. Meas. Tech., 8, 2251–2266, https://doi.org/10.5194/amt-8-2251-2015, 2015.

Pentikäinen, P., O'Connor, E. J., Manninen, A. J., and Ortiz-Amezcua, P.: Methodology for deriving the telescope focus function and its uncertainty for a heterodyne pulsed Doppler lidar, Atmos. Meas. Tech., 13, 2849–2863, https://doi.org/10.5194/amt-13-2849-2020, 2020.

Petters, M. D., Pujiastuti, T., Rasheeda Satheesh, A., Kasparoglu, S., Sutherland, B., and Meskhidze, N.: Wind-driven emissions of coarse-mode particles in an urban environment, Atmos. Chem. Phys., 24, 745–762, https://doi.org/10.5194/acp-24-745-2024, 2024.

Platt, C. M., Young, S. A., Carswell, A. I., Pal, S. R., McCormick, M. P., Winker, D. M., DelGuasta, M., Stefanutti, L., Eberhard, W. L., Hardesty, M., Flamant, P. H., Valentin, R., Forgan, B., Gimmestad, G. G., Jäger, H., Khmelevtsov, S. S., Kolev, I., Kaprieolev, B., ren Lu, D., Sassen, K., Shamanaev, V. S., Uchino, O., Mizuno, Y., Wandinger, U., Weitkamp, C., Ansmann, A., and Wooldridge, C.: The Experimental Cloud Lidar Pilot Study (ECLIPS) for Cloud–Radiation Research, Bull. Amer. Meteor. Soc., 75, 1635 – 1654, https://doi.org/10.1175/1520-0477(1994)075<1635:TECLPS>2.0.CO;2, 1994.

Warren, E., Charlton-Perez, C., Lean, H., Kotthaus, S., and Grimmond, S.: Spatial variability of forward modelled attenuated backscatter in clear-sky conditions over a megacity: Implications for observation network design, Quart. J. Roy. Meteor. Soc., 148, 1168–1183, https://doi.org/doi.org/10.1002/qj.4253, 2022.

Westbrook, C. D., Illingworth, A. J., O'Connor, E. J., and Hogan, R. J.: Doppler lidar measurements of oriented planar ice crystals falling from supercooled and glaciated layer clouds, Quart. J. Roy. Meteor. Soc., 136, 260–276, https://doi.org/https://doi.org/10.1002/qj.528, 2010.

https://doi.org/10.5194/egusphere-2026-1140
Preprint. Discussion started: 5 May 2026


Wiegner, M. and Geiß, A.: Aerosol profiling with the Jenoptik ceilometer CHM15kx, Atmos. Meas. Tech., 5, 1953–1964, https://doi.org/10.5194/amt-5-1953-2012, 2012.

https://doi.org/10.5194/egusphere-2026-1140
Preprint. Discussion started: 5 May 2026


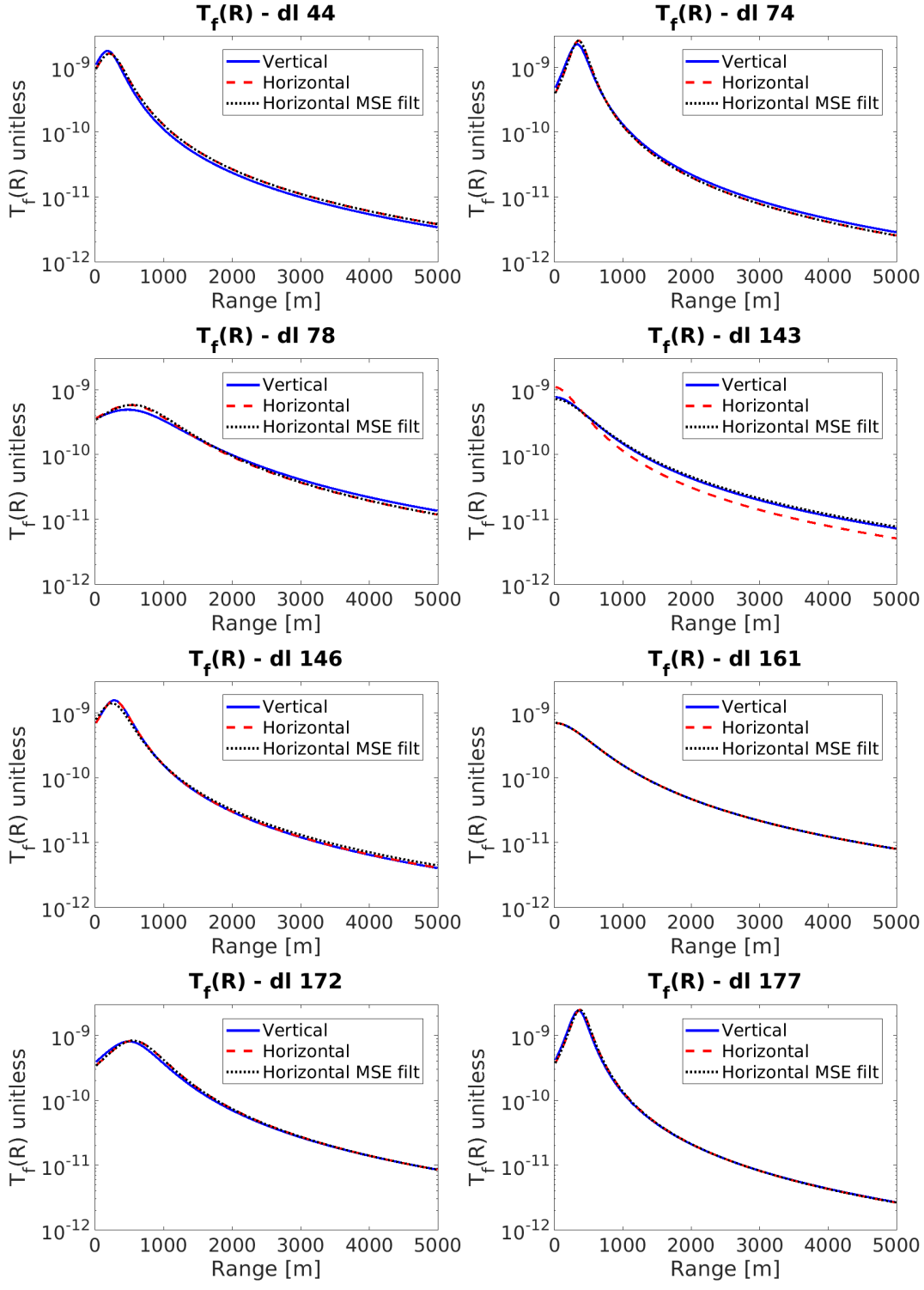


**Figure 2.** $T_f$ for all Doppler lidars estimated with the vericatical, horizontal and horizontal MSE filtered methods.

https://doi.org/10.5194/egusphere-2026-1140
Preprint. Discussion started: 5 May 2026


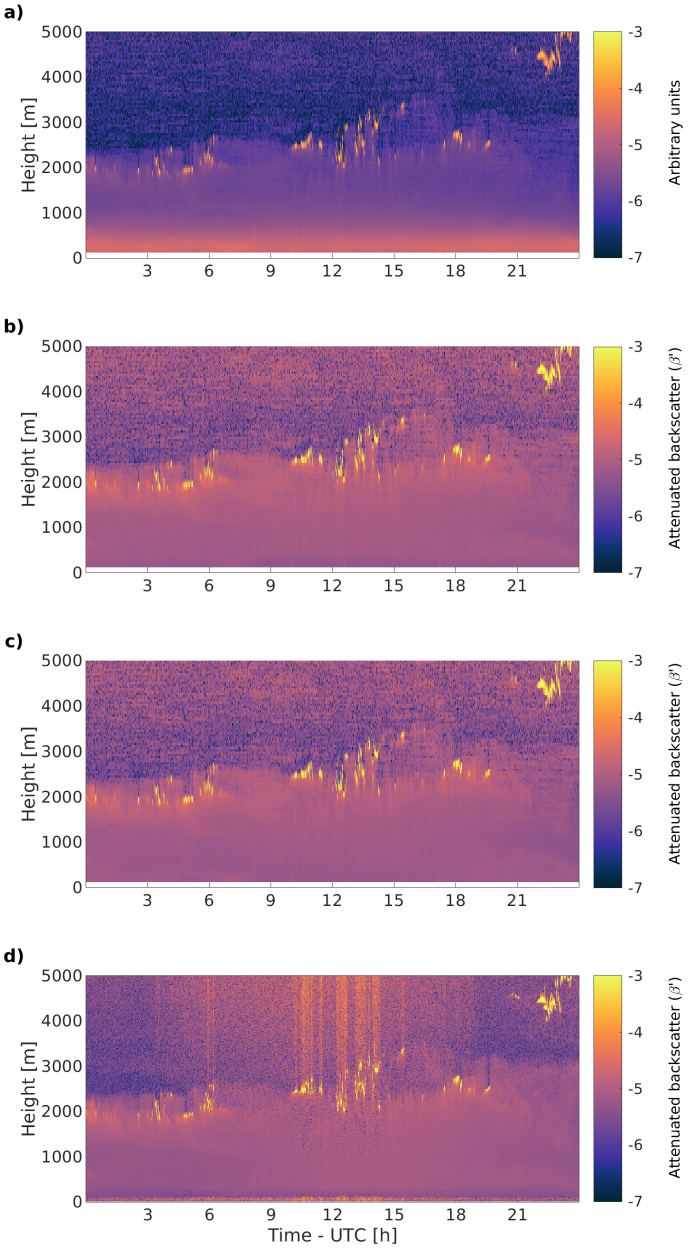


**Figure 3.** a) Doppler lidar attenuated backscatter calculated with the original assumption of $T_f(R)$. b) Doppler lidar backscatter calculated with $T_f(R)$ obtained using the vertical method. c) Doppler lidar backscatter calculated with $T_f(R)$ obtained using the horizontal MSE filtered method. d) Attenuated backscatter from the CHM15k ceilometer. Data from 24th July 2021. Doppler lidar data from unit number 44.

https://doi.org/10.5194/egusphere-2026-1140
Preprint. Discussion started: 5 May 2026


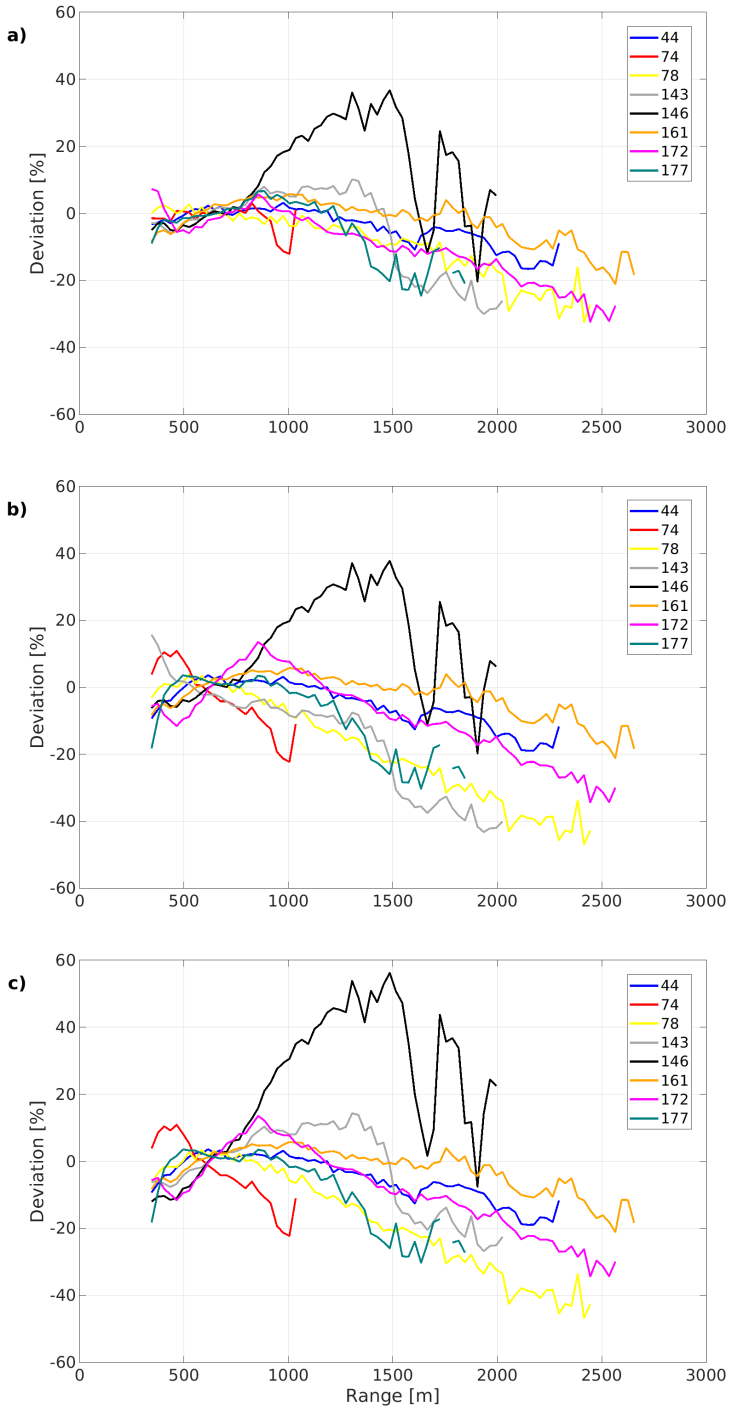


**Figure 4.** Median deviation between ceilometer attenuated backscatter profiles and Doppler lidar attenuated backscatter profiles during 24-25 July 2021. The deviation are normalized between of 345 m and 885 m. Doppler lidar attenuated backscatter is calculated based on $T_f$ from a) vertical method, b) horizontal method, and c) horizontal MSE filtered method.

https://doi.org/10.5194/egusphere-2026-1140
Preprint. Discussion started: 5 May 2026


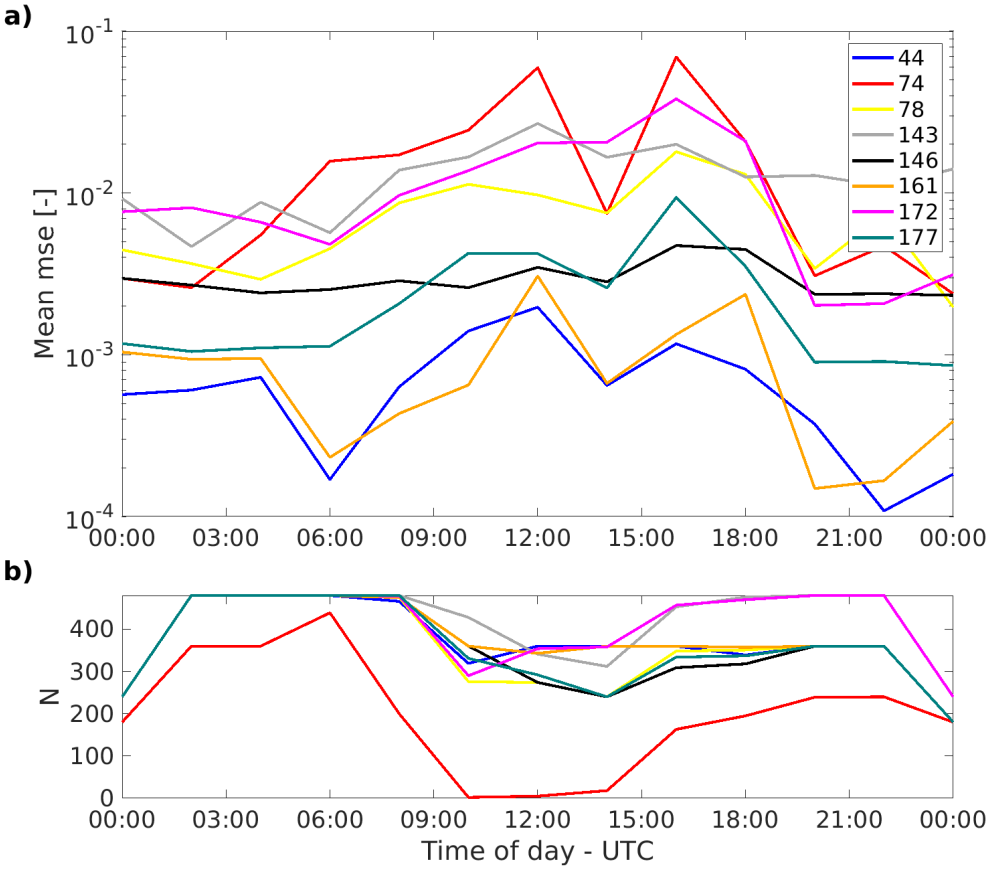


**Figure 5.** a) MSE between unity and normalized near horizontal SNR profiles corrected with the best estimate of horizontal MSE filtered $T_{\mathrm{f}}(R)$ as a function of time of day for all 8 Doppler lidars for the period 24-25 July 2021. b) Number of profiles available for deriving $T_{\mathrm{f}}(R)$ for each time step for each Doppler lidar.